JEM

Supplemental material

Fenwick et al., https://doi.org/10.1084/jem.20182359

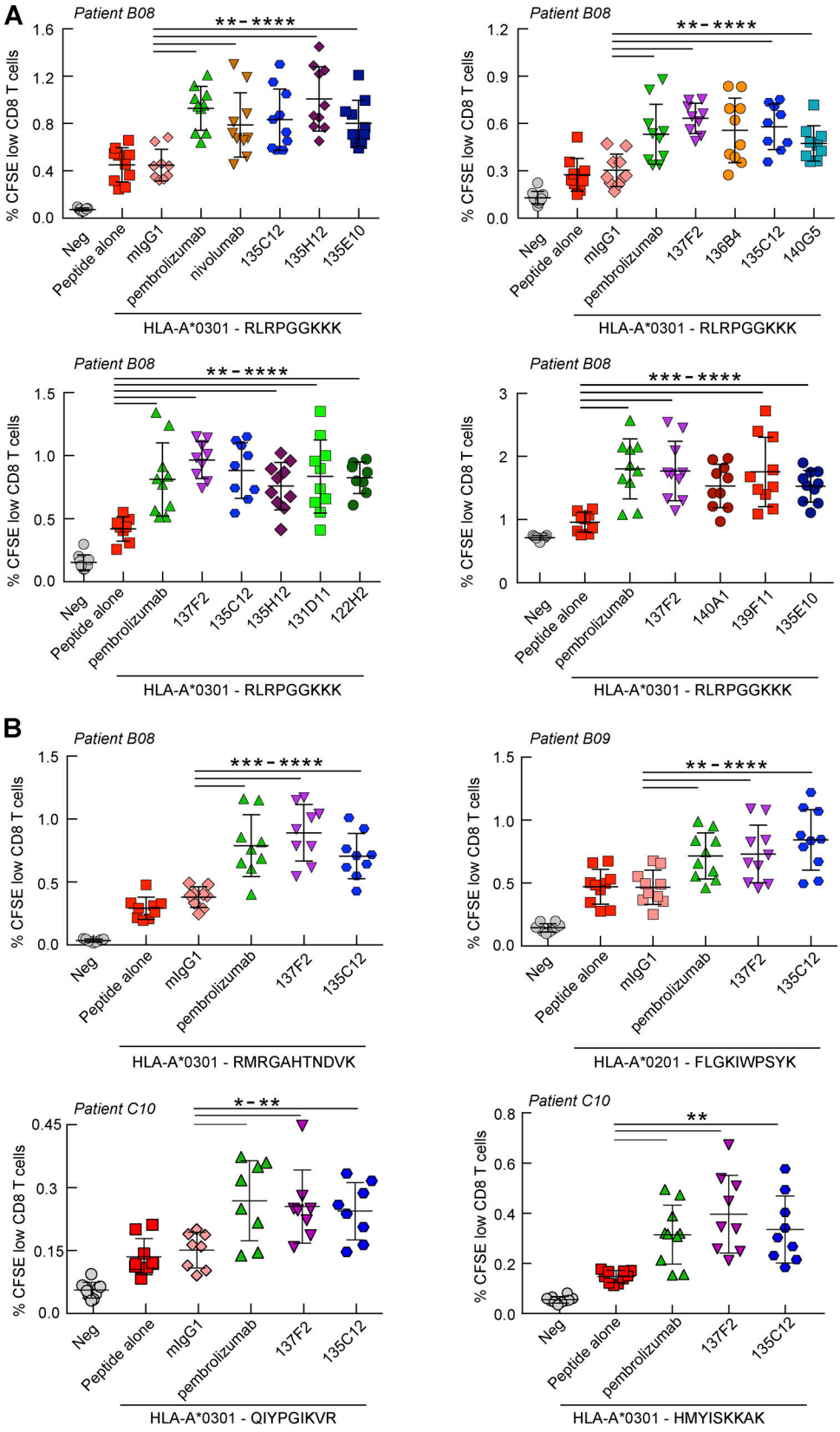

Figure S1. **Enhancement of proliferation of Ag-specific exhausted CD8 T cells by a panel of prioritized anti–PD-1 Abs. (A)** Effects of the prioritized set of anti–PD-1 Abs on the recovery of the proliferation of HIV-specific CD8 T cells. Blood mononuclear cells from an HIV-positive donor were labeled with CFSE and stimulated with the specific HIV-derived peptide in the presence or absence of an anti–PD-1 Ab for 6 d. **(B)** Select Abs were further analyzed using different HIV-derived peptides and in two different patients. Untreated samples (Neg) were used as a negative control in each experiment. Graphs show the mean ± SD. **, P < 0.0029; ***, P < 0.0006; ****, P < 0.0001 (unpaired *t* test with Welch's correction).

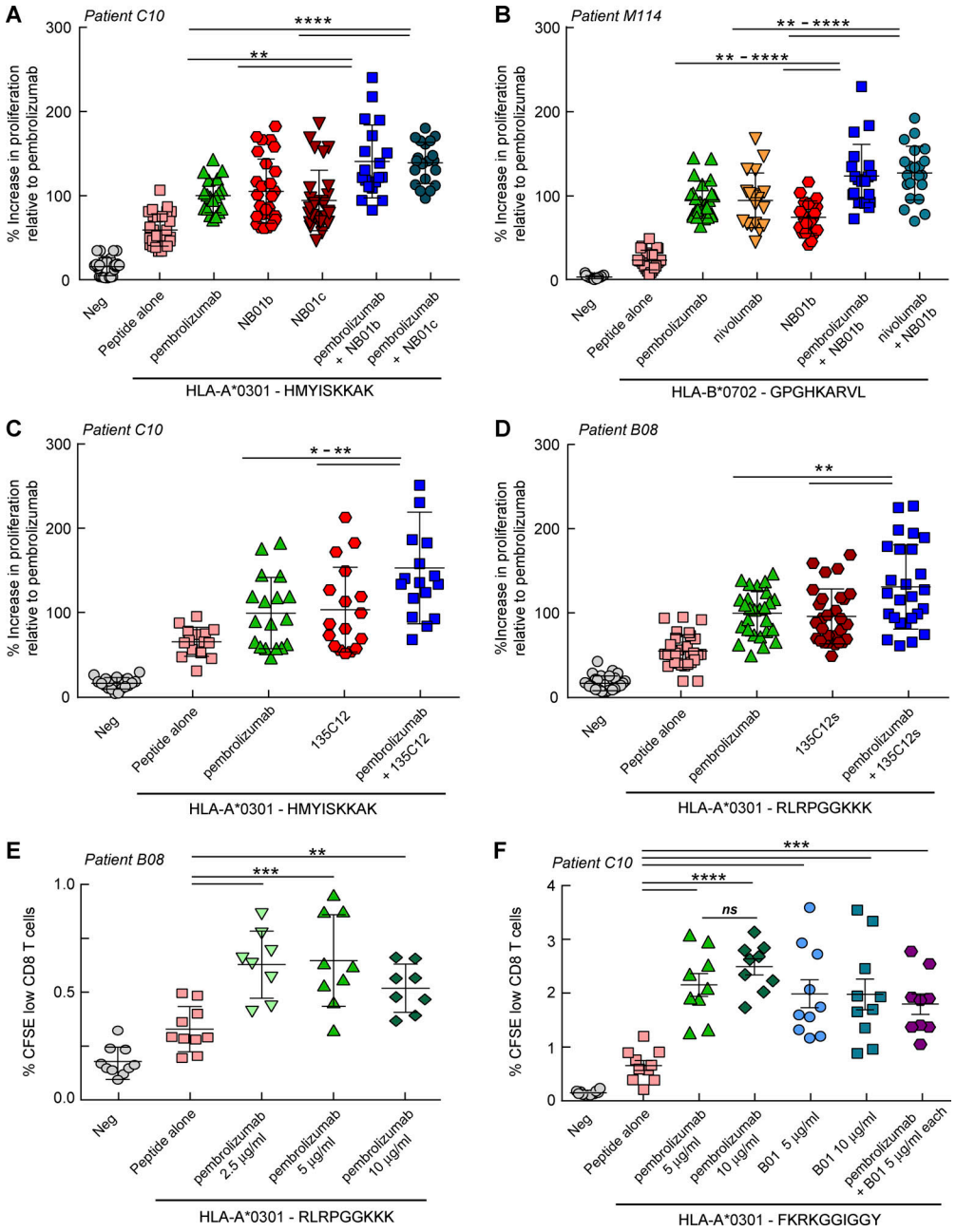

Figure S2. **Blocking and nonblocking anti–PD-1 Abs combinations synergize in recovering the proliferation of exhausted Ag-specific CD8 T cells. (A–D)** Enhanced Ag-specific proliferation of CD8 T cells is observed in the in vitro CFSE functional exhaustion assay upon treatment with combinations of a blocking anti–PD-1 Ab (pembrolizumab or nivolumab) and a nonblocking anti–PD-1 Ab (NB01b or NB01c Abs in A, NB01b Ab in B, 135C15 mouse Ab in C, and a 135C12 mouse sibling Ab in D). The data shown are an average of two independent experiments and show a statistically significant increase in CD8 T cell proliferation. **(E)** Effect of different concentrations of anti–PD-1 Abs in the in vitro functional recovery CFSE assay shows maximum enhancement of CD8 T cell proliferation induced by pembrolizumab at 5 µg/ml, with no significant improvement at higher doses. **(F)** Lack of evidence of synergy using combinations comprising two blocking anti–PD-1 Abs (pembrolizumab + B01) used at 5 µg/ml each. ANOVA performed between the individual Abs and Ab combinations confirmed a statistical difference with the Ab combination therapy. Untreated samples (Neg) were used as a negative control in each experiment. Graphs show the mean ± SD. ns, not significant; *, P < 0.02; **, P < 0.0086; ***, P < 0.0006; ****, P < 0.0001 (unpaired *t* test with Welch's correction).

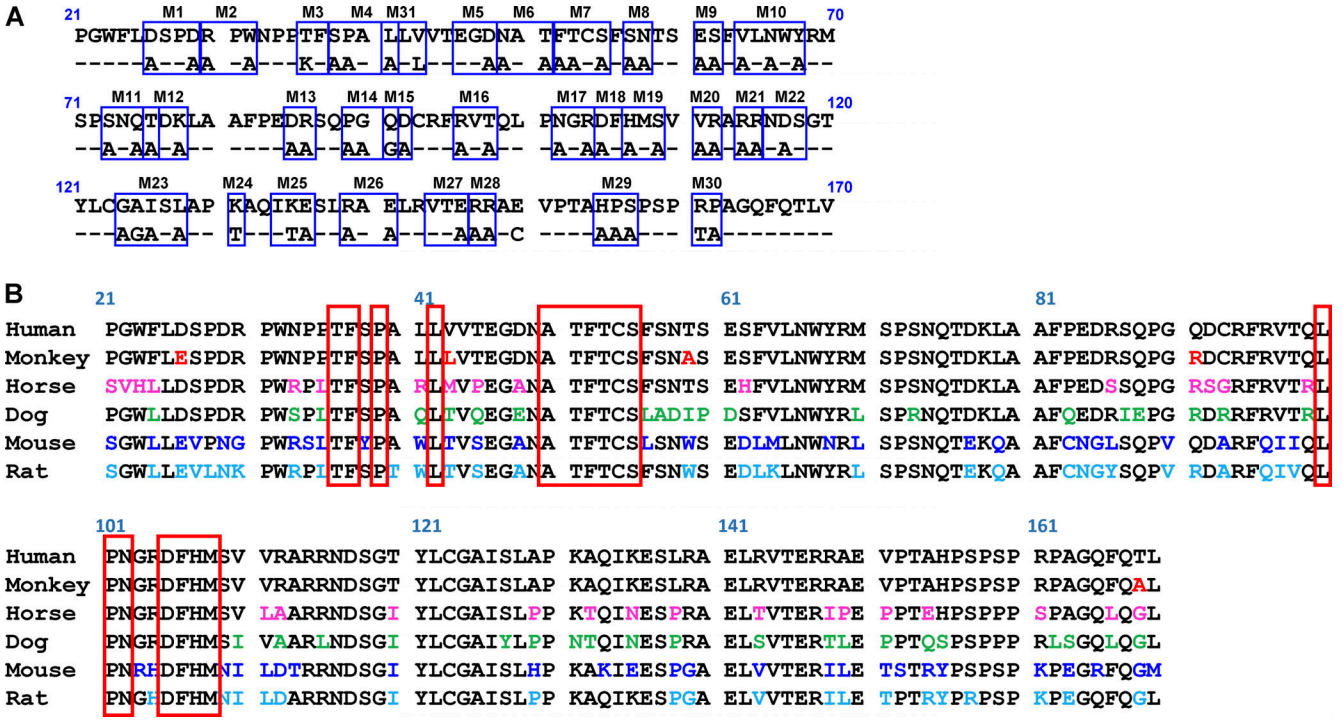

Figure S3. **PD-1 sequence map of mutations used for Ab epitope mapping and sequence alignment of PD-1 from different species. (A)** Site-directed mutagenesis studies performed with human PD-1 constructs with discrete amino acid substitutions at solvent-accessible residues of the ectodomain that were designed to map the binding of anti–PD-1 Abs to PD-1 expressed at the surface of transiently transfected HeLa cells. The M32 mutation was generated with substitutions L41A/V43T/S137A/L138A/R139T after observing a small reduction in binding of the 135C12 Ab to PD-1 expressed from the M26 and M31 vectors. **(B)** Amino acid sequence alignment of the ectodomains for human, monkey, dog, horse, mouse, and rat PD-1 proteins. The different species are 96.6% (monkey), 72.5% (dog), 79.2% (horse), 61.7% (mouse), and 66.4% (rat) identical compared with human PD-1. Residues outlined in red boxes come together at the surface of PD-1 to form the P1 conserved patch that partially overlaps with the binding epitopes for 135C12/NB01 and 136B4 Abs. These Abs were demonstrated to bind monkey PD-1, but no specific binding could be detected with cell-surface mouse PD-1, indicating that residues outside the P1 patch are also important for high-affinity binding.

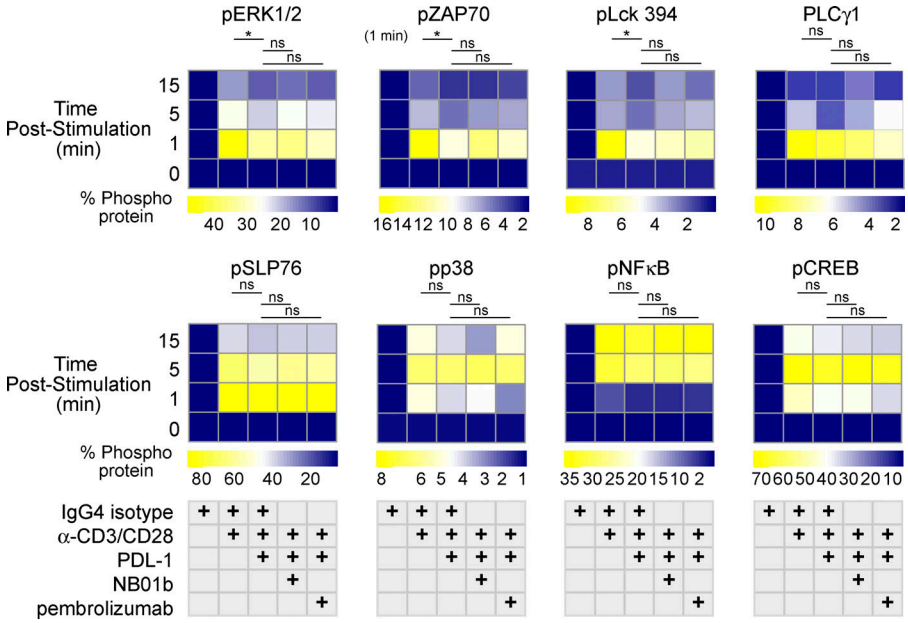

Figure S4. **PD-1–PDL-1–mediated suppression in phosphosignaling following stimulation of exhausted T cells.** Heatmap of mean phosphorylation levels in CD45RA$^-$ memory T cells treated with (1) IgG4 isotype control Ab, (2) IgG4 control + anti-CD3/CD28 Abs, (3) anti-CD3/CD28 Abs + PDL-1 Fc fusion protein, (4) anti-CD3/CD28 Abs + PDL-1 Fc fusion protein + NB01b, and (5) anti-CD3/CD28 Abs + PDL-1 Fc fusion protein + pembrolizumab. Significant suppression of T cell signaling mediated through PDL-1 was observed for AKT pT308, AKT pS473, PDK1 pS421, and ERK1/2 pT202/pY204 at the 5- to 15-min time points. ZAP70 pY319 and Src pY418/Lck pY394 showed significant PDL-1–mediated suppression only at the 1-min time point after stimulation. Additional phosphoproteins at different time points showed trends toward PDL-1 mediated suppression or anti–PD-1–mediated relief of exhaustion. However, these failed to meet statistical significance in our studies (n = 4–8 experiments for the different phosphoproteins). False discovery rate–corrected Student's t tests were used to evaluate the statistical difference between the treatment conditions. ns, not significant; *, $P < 0.05$ for the indicated comparisons.

Table S1. **X-ray data statistics for the hPD-1–NB01a Fab complex**

	hPD-1–Fab A35774 complex
X-ray source	Beamline ID29, ESRF (Grenoble, France)
Detector	Pilatus 6M (Dectris)
Wavelength (Å)	0.97625
Space group	$P\ 1\ 2_1\ 2$
Cell dimensions (Å)	A = 64.5, b = 63, c = 68.3
	α, γ = 90, β = 106°
Resolution range (Å)	65.49–2.20 (2.27–2.20)
Number of unique reflections	26,237 (2,621)
R_{merge} (%)	6.96 (52.0)
R_{meas} (%)	8.54 (64.5)
Average $I/\sigma(I)$	10.77 (2.16)
Completeness (%)	97.59 (98.28)
Multiplicity	2.9 (2.7)
CC (1/2)	0.997 (0.711)
Wilson B-factor (truncate; Å^2)	33.88
Solvent content (%)	40.39
Number of reflections used in refinement	26,236 (2,621)
Number of reflections used for R_{free}	1,265 (143)
R_{work} (%)	21.48 (28.57)
R_{free} (%)	26.97 (37.04)
Rms bond length (Å)	0.002
Rms bond angle (°)	0.49
Ramachandran favored (%)	96.86
Ramachandran allowed (%)	2.73
Ramachandran outliers (%)	0.42
Clash score	2.97

CC, Pearson's correlation coefficient; Rms, root mean square.